Appl. Phys. A (2017) 123:190
DOI 10.1007/s00339-017-0826-4

Applied Physics A
Materials Science & Processing

Generation of NiO nanoparticles via pulsed laser ablation in deionised water and their antibacterial activity

Khawla S. Khashan[1] · Ghassan M. Sulaiman[2] · Abubaker H. Hamad[3] · Farah A. Abdulameer[1] · Assel Hadi[1]

Received: 10 August 2016 / Accepted: 31 January 2017 / Published online: 25 February 2017

Abstract Nickel oxide (NiO) nanoparticles were synthesised by nanosecond laser ablation in deionised water. Spherical NiO nanoparticles with sizes ranging from 2 to 21 nm were produced. The optical absorption spectra of the nanoparticles were measured using UV–VIS spectroscopy, and their size distribution was characterised using transmission electron microscopy (TEM). The crystalline material structures were investigated using X-ray diffraction (XRD). Fourier transform infrared spectroscopy (FTIR) was used to obtain infrared spectra of the samples. The results show that crystalline NiO nanoparticles were produced. The antibacterial activity of the nanoparticles against *Escherichia coli, Pseudomonas aeruginosa, Proteus vulgaris*, and *Staphylococcus aureus* bacteria was then examined. It was found that the NiO nanoparticles have a synergistic effect on inhibiting *E. coli* and *S. aureus* growth; this effect was also tested using the well-diffusion method. In this method, NiO nanoparticles at a concentration of 1000 μg ml^{-1} along with amoxicillin yielded an inhibition zone against *E. coli* of 14.3 ± 1.15 mm; this zone was 12.6 ± 0.57 mm against *S. aureus*. Therefore, from the present findings, it can be concluded that the efficiency of inhibiting bacterial growth could be improved by the addition of metal-oxide nanoparticles to amoxicillin in comparison with either pure amoxicillin or pure metal-oxide nanoparticles.

✉ Khawla S. Khashan
khawla_salah@yahoo.com

[1] Division of Laser Physics, Department of Applied Science, University of Technology, Baghdad, Iraq

[2] Division of Biotechnology, Department of Applied Science, University of Technology, Baghdad, Iraq

[3] General Science Department, Faculty of Education, Soran University, Soran, Erbil, Kurdistan Region, Iraq

1 Introduction

Nanoparticles have unique electronic, optical, chemical, and biological properties compared with bulk materials [1]. For example, the electrical conductivity, electrical resistivity, strength and hardness, diffusivity, chemical reactivity, and biological activity of nanoparticles are different from their bulk counterparts [2]. Therefore, nanoparticles are promising candidates for many applications, such as heterogeneous catalysis, gas-sensor technology, photovoltaics, microelectronics, nonlinear optics, and medicine [3–6]. A wide variety of techniques have been developed to produce those nanoparticles, such as pulsed laser deposition [7], sol–gel [8], spray pyrolysis [9], solvothermal method [10], surfactant-mediated synthesis [11], chemical method [12], and laser ablation methods [1]. Pulsed laser ablation in liquids (PLAL) is a facile single-step top-down technique used to synthesis nanoparticles. This technique has several advantages over traditional methods, among which are the ability to control the size and properties of the nanoparticles produced and the ability to ensure that they are free of contamination. In addition, it is used for preparing different nanostructure materials [13–15].

The size, shape, and morphology of the nanoparticles produced by laser ablation in liquid depend critically on several ablation parameters, such as laser fluence, pulse width, repetition rate, temperature, ablation time, wavelength, the level of the liquid above the target surface, and, when used, the concentration of the stabilising agent [16]. Nano-structured nickel oxide (NiO) has a large exciting binding energy and a large bandgap ranging from 3.6 to 4.0 eV [17]. This semiconductor can be utilised in optical, electronic, catalytic, and super-paramagnetic devices, such as transparent conductive films, gas sensors, and dye-sensitised solar cells [18]. A concourse between the

nanotechnology and biology can resolve several biomedical problems and can find materials with nanoscale diameters that have enhanced bioactivity. Due to their enhanced effectiveness, new nanoparticle drugs composed of polymers, metals, metal oxides, or ceramics can combat cancer and fight human pathogens like bacteria [19]. Metal-oxide nanoparticles can be used as antimicrobial agents because of their effectiveness on resistant strains of microbial pathogens, as well as their low toxicity and heat resistance [20]. Among these nanoparticles, NiO nanoparticles display the highest antimicrobial activities. This is related to the fact that Ni^{2+} has the highest toxicity to cells and the small size of NiO particles could enhance their solubility. Furthermore, the presence of extracellular Ni^{2+} has the potential to interfere with the intracellular Ca^{2+} metabolism and causes cellular damage [21]. The bactericidal property of such nanoparticles depends on their size, stability, and the concentration added to the growth medium, which provides greater retention time for interaction between the bacterium and the nanoparticles [22].

In this paper, the authors investigated the effect of changing ablation time and laser energy on synthesised NiO nanoparticles by laser ablation in liquid. The antibacterial activities of these nanoparticles with or without amoxicillin on cultures of Gram-negative and Gram-positive bacteria were also tested.

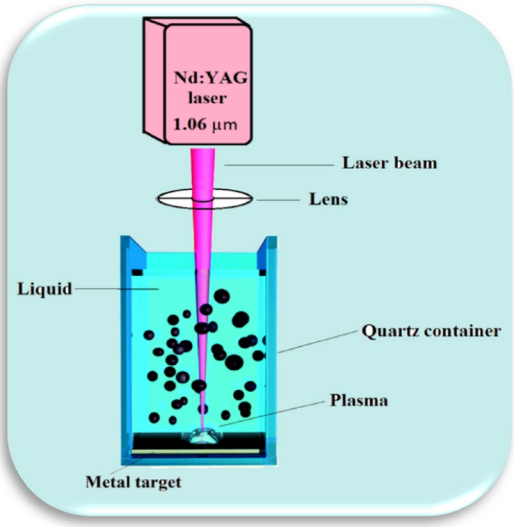

Fig. 1 Experimental setup for synthesis of NiO nanoparticles by laser ablation in liquid

2 Experimental methods

2.1 NiO nanoparticle production

NiO nanoparticles were synthesised by laser ablation of a nickel metal pellet (1.5 cm in diameter and 3 mm in thickness) in deionised water. As shown in Fig. 1, the target was placed at the bottom of a quartz vessel containing 1 ml of deionised water; the water level above the target was about 2 mm. A pulsed Q-switched Nd:YAG nanosecond laser was used to produce the nanoparticles with the following parameters: wavelength $\lambda = 1064$ nm, frequency $f = 1$ Hz, and pulse width $\tau = 9$ ns, at different laser energies (40–200 mJ/pulse). The ablation time varied from 5 to 20 min. A microbalance scale was used to determine the mass concentration of the colloidal nanoparticles by weighing the bulk target before and after the nanoparticle production process.

2.2 Nanoparticle sample preparation for characterisation

For TEM analyses, a copper micro-grid mesh (gold-coated copper grid −200 meshes) was used for the sample preparation. After depositing a drop of colloidal nanoparticles onto the mesh, the substrate was allowed to dry at room temperature. The X-ray diffraction sample was prepared via depositing colloidal nanoparticles on an aluminum substrate by the drop casting technique.

2.3 Characterisation of nanoparticles

To characterise the nanoparticles, a double-beam UV–Vis spectrophotometer (SP-3000 Plus, OPTIMA) was used for examining the absorption spectra of the colloidal nanoparticles within the spectral range (200–500 nm). A Transmission Electron Microscope (TEM) (Philips EM 208S) was used to examine the morphology of the nanoparticles and measure their size and size distribution. Fourier transform infrared (FTIR) spectroscopy (8000 Series, Shimadzu) was used in the spectral range of 400–4000 cm^{-1} to study the molecular vibrations of the nanoparticles. X-ray diffraction (XRD) (Philips PW) with a Cu-Kα radiation source at $2\theta = (30–60)$ degrees was used for the investigation of the crystalline material structures. The grain size was calculated using the Scherrer formula [23]:

$$D = 0.94\,\lambda\,/\beta\cos\theta, \tag{1}$$

where λ is the X-ray wavelength (1.54060 Å), β is the full-width at half maximum of the diffraction line in radians, and θ is the diffraction angle.

An optical spectrophotometer was used to measure the optical density of the bacterial cultures in a liquid medium at 600 nm (OD_{600}).

2.4 Antibacterial activity analysis

The antibacterial activities of the nanoparticles were tested against *Escherichia coli, Pseudomonas aeruginosa, Proteus vulgaris* (gram-negative bacteria), and *Staphylococcus aureus* (gram-positive bacteria) using a liquid medium method. The bacteria suspension was prepared by adjusting the tubes to a 0.5 McFarland turbidity standard (5×10^7 cell mL^{-1}) tubes. Each bacterial strain was subcultured in a nutrient broth.

To investigate the inhibition rate, the broth was inoculated with 0.2 ml of bacterial strains, and then with 0.5 ml in solutions of 400, 600, or 1000 µg ml^{-1} of concentration of NiO nanoparticles without antibiotics (amoxicillin at a concentration of 30 µg ml^{-1}) or a combination after vortex mixing. The tubes were incubated at 37 °C for 24 h. Bacterial growth was measured by optical density at 600 nm wavelength. The mean values of the inhibition were calculated from taking a triple reading of each test. A broth tube containing bacterial strains only (without nanoparticles) was used as a control. Inhibition efficiency (%) was expressed using the UV spectrophotometer model (APEL PD-303) JAPAN as follows [24]:

$$\text{Inhibition efficiency (\%)} = \left((\text{control OD}_{600} - \text{test OD}_{600})/\text{control OD}_{600}\right) \times 100\%. \quad (2)$$

The effect of the nanoparticles at different concentrations combined with amoxicillin was also determined using the well-diffusion method against *E. coli* and *S. aureus*. A lawn of bacterial culture was spread on the nutrient agar plates, and the plates were allowed to rest for 10–15 min to allow culture absorption. Wells measuring 8 mm in size were punched into the agar with the tip of a sterile micropipette. Using a micropipette, the nanoparticle solutions at concentrations of 400, 600, or 1000 µg ml^{-1} combined with amoxicillin were poured into the wells. After incubation at 35 ± 2 °C for 24 h, the inhibition zone diameter was measured. The antibiotic amoxicillin was used as a control.

2.5 Statistical analysis

The data were statistically evaluated using ANOVA and a one-tailed unpaired Student's *t* test for significance testing, where $p < 0.05$ was considered significant. Values are presented as the mean ± SD of the three replicates of each experiment.

3 Results and discussion

Transmission electron microscopy (TEM) was used to determine the size distribution and morphology of nanoparticles. Figure 2a shows a TEM image of NiO nanoparticles prepared at 200 mJ for an ablation time of 10 min, while Fig. 2b shows the size distribution. NiO nanoparticles with a diameter in the range of 2–21 nm and spherical shape were obtained. These were aggregated strongly due to the electrostatic attractive force between nanoparticles produced by the electric double layer on the nanoparticles' surfaces [25]. The nanoparticles are charged in liquid. An electrical layer surrounds the surface of the nanoparticles as a result of the interaction between the liquid molecules and the surface-charged nanoparticles [1]. It is worth mentioning that interaction between the plasma plume and nanoparticles can take place, which depends on the attractive and repulsive forces between the plume species and

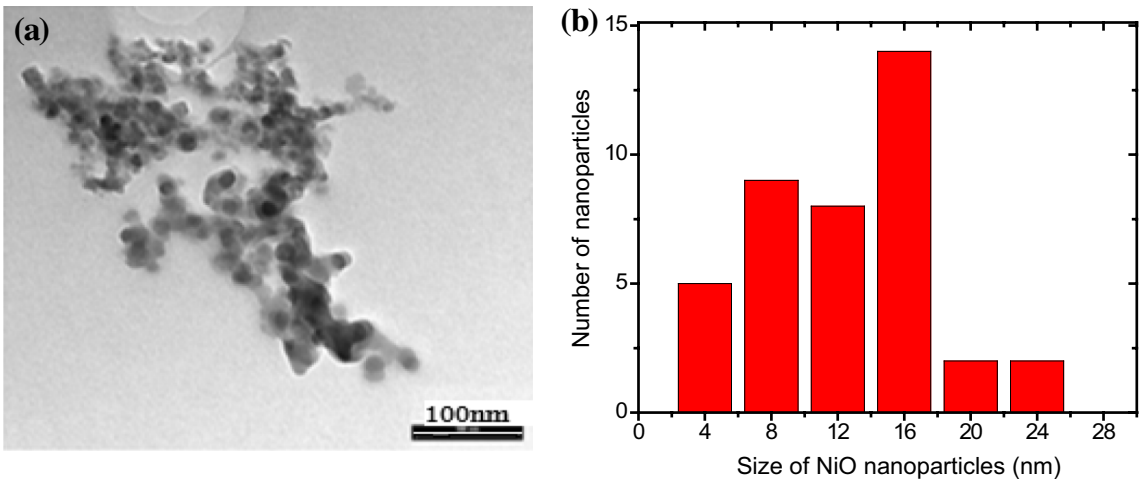

Fig. 2 TEM image (**a**) and size distribution (**b**) of NiO nanoparticles prepared by laser ablation in deionised water

nanoparticles. These forces, such as attractive Van der Waals force, may cause growth and/or aggregation.

The colour of the colloidal NiO nanoparticles prepared by laser ablation in deionised water at different conditions changed from light grey to dark grey. This transformation is because of the oscillation of the conduction band electrons in the nanoparticles, known as surface plasmon oscillation; this phenomenon is stimulated by incident light. In other words, the resonance condition, known as surface plasmon resonance (SPR), occurs when the frequency of the light photons matches the natural frequency of the nanoparticles′ surface electrons. The colour intensity of the solution increased with increasing laser energy and ablation time due to the increase in the concentration of nanoparticles in the colloid.

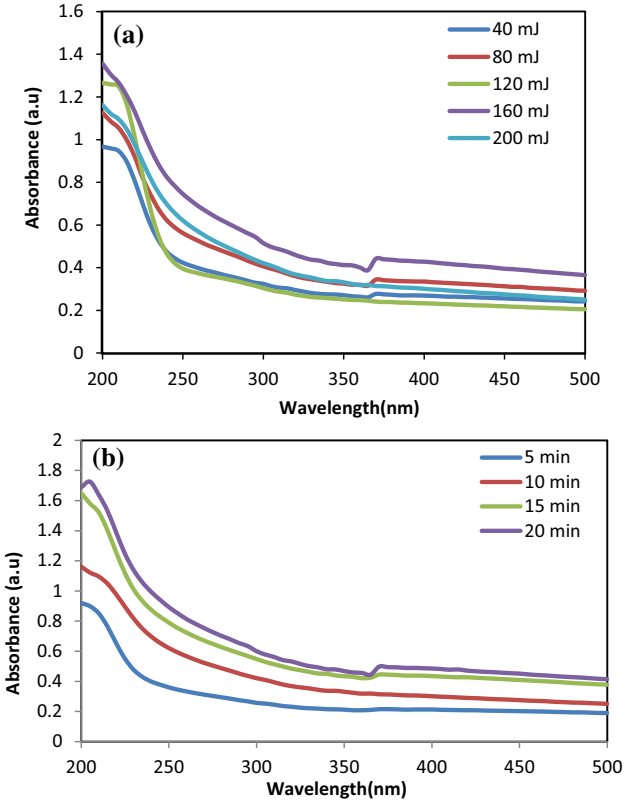

Fig. 3 UV–VIS absorption spectra of NiO nanoparticles prepared by laser ablation in deionised water: **a** at different laser energies for 10 min; **b** at 200 mJ for different ablation times

Figure 3 shows the optical absorption spectrum of the NiO nanoparticles prepared at different laser energies (40, 80, 120, 160, and 200 mJ) for a constant ablation time (10 min) and at a constant laser energy (200 mJ) for different ablation times (5, 10, 15, and 20 min). As shown in Fig. 3a, the absorption spectrum exhibits broad bands whose absorption decreases continuously above 210 nm. The optical absorption edges also shifted slightly towards longer wavelengths (red shift) due to the increase in particle size [26]. Delivering more energy to the target means ablating larger amounts of material and producing an intense plasma plume, so that the colloidal nanoparticles become denser. The absorbance of the NiO nanoparticles in deionised water has almost increased consistently with the ablation time of the target material. The change in absorbance indicates that the number density of the nanoparticles increased with increasing ablation time. These results agree with those reported in [27], while the second weaker peak was due to change the wavelength from the UV region to VIS region.

Figure 4a shows the influence of laser energy on the mass concentration of NiO nanoparticles. It can be seen that the concentration of the nanoparticles increased with increasing laser energy, which may be attributed to increased evaporation of the target at an increased surface

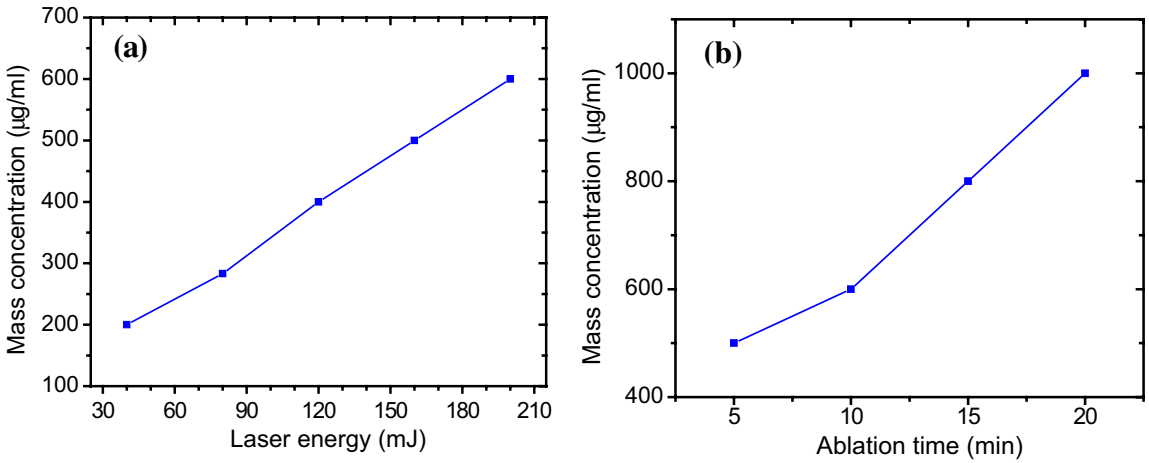

Fig. 4 Mass concentration as a function of **a** laser energy and **b** ablation time

temperature caused by increased laser energy. The production rate depends on some factors related to the optical and thermal properties of the target, such as the reflectivity, light absorbance of the target surface, heat capacity, enthalpy of vaporisation, boiling point, and thermal conductivity of the target [28]. The effect of the ablation time on the concentration of nanoparticles at the laser energy of 200 mJ is shown in Fig. 4b. The mass concentration increased with increasing ablation time. The increase in ablation time causes the production of a higher concentration of particles, but it was also saturated because of the high concentration of light absorption in the colloidal nanoparticles. It has been reported that the ablation efficiency of the nanoparticles decreases with ablation time, which may be due to the presence of nanoparticles in liquid, which could interact with the laser beam and decrease the power delivered to the metal surface. Conversely, changes to the metal surface by laser irradiation could reduce the ablation efficiency [27].

FTIR measurements were recorded to confirm the formation of oxide bonds for NiO nanoparticles. In general, the absorption bands of the metal-oxide nanoparticles are below 1000 cm^{-1}, arising from inter-atomic vibrations [29]. Figure 5a, b shows the FTIR of the NiO colloidal nanoparticles prepared at laser energies of 80 and 200 mJ for a 10 min ablation time. The peaks at 491 cm^{-1} correspond to the stretching vibration mode of the Ni–O bond. The broad peaks at 3420 cm^{-1} correspond to the band O–H stretching vibrations and the peak near 1641.3 cm^{-1} is assigned to the H–O–H bending vibration mode. The intensity of the FTIR spectrum changes with a change in laser energy, while the width of the peaks is constant. These results are in agreement with the data reported in [30]. The region around 2090 cm^{-1} is assigned to the C–O molecules [31].

Figure 6 shows XRD of the crystalline phase of the nanoparticles generated at 200 mJ for 10 min. The peaks centred at $2\theta = 37.25°$ and 43.2° correspond to the 111 and 200

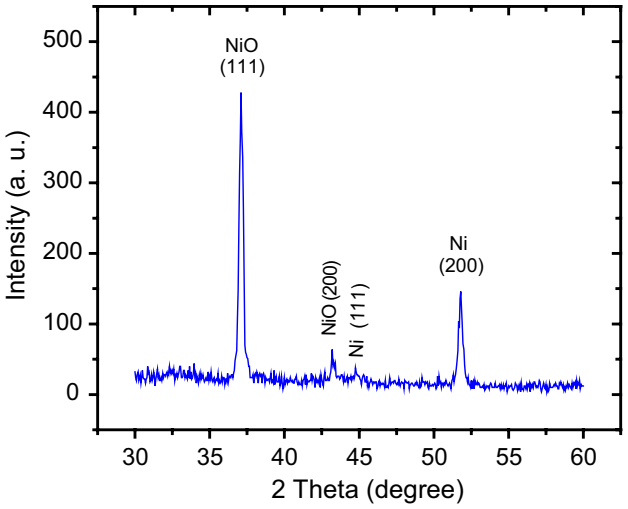

Fig. 6 XRD pattern resulting from NiO nanoparticles prepared by 1064 nm laser ablation at 200 mJ for 10 min

phases that are assigned to the crystal planes of the nickel oxide phase [28]. The peaks at $2\theta = 44.45°$ and 51.8° correspond to 111 and 200, which match the nickel [32], this peak related to incompleteness chemical reactions between the ejected Ni and the surrounding liquid in the process of NP formation. The grain size (D) values, calculated with Scherrer's equation using Eq. (1), are shown in Table 1.

Figure 7a shows the optical density of *E. coli, S. aureus, P. aeruginosa, and P. vulgaris*, cultured in Lysogeny broth (LB) media in the presence of NiO nanoparticles. It can be noted that the optical density at 600 nm (OD_{600}) dropped slightly when the concentrations of the nanoparticles increased. This means that the inhibitory effect of the nanoparticles was dependent upon the concentration. As shown in Fig. 7b, the 1000 µg ml^{-1} concentration was the best concentration of NiO nanoparticles for inhibiting growth of both Gram-positive and Gram-negative strains.

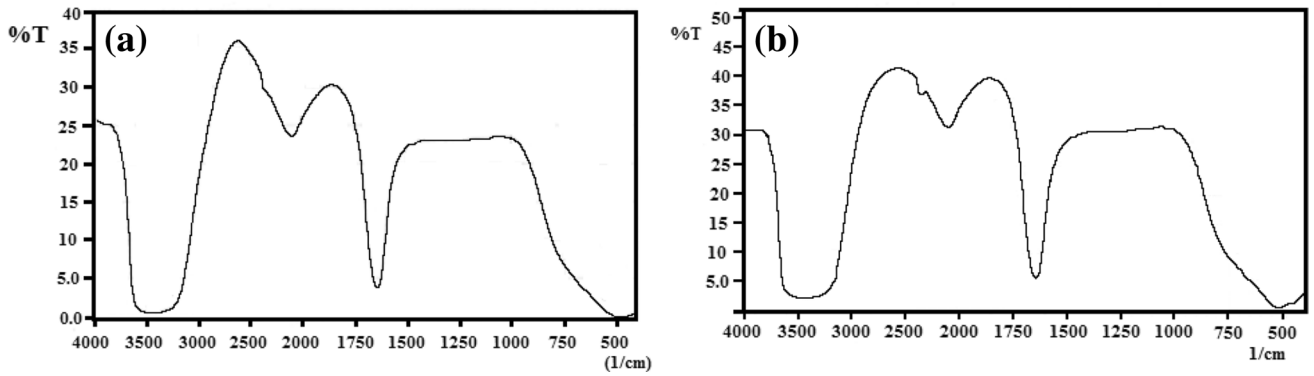

Fig. 5 FTIR spectrum of NiO nanoparticles prepared by laser ablation of nickel in deionised water at **a** 80 mJ for 10 min and **b** 200 mJ for 10 min

Table 1 XRD parameter investigation for NiO nanoparticles

Ablation condition	2θ (°)	Orientation (hkl)	G.S (nm)	FWHM (°)	Type
200 mJ 10 min	37.25	111	33.75	0.2482	NiO
	43.2	200	47.63	0.1793	NiO
	44.45	111	25.91	0.3310	Ni
	51.8	200	34.59	0.2551	Ni

The inhibition rate of the nanoparticles at a concentration of 1000 µg ml^{-1}, calculated from Eq. (2), was 26, 25.9, 18.8, and 26.7% of *E. coli, S. aureus, P. aeruginosa*, and *P. vulgaris*, respectively. It can be seen that at this concentration, *P. vulgaris* is more affected than the other types of bacteria, while *P.aeruginosa* seemed to be more resistant to NiO nanoparticle than Gram-negative bacteria. However, the antibacterial activity of NiO nanoparticles was approximately similar in Gram-negative bacteria to those observed of Gram-positive bacteria. The interaction between NiO nanoparticle surface and the cell wall constituents might have caused structural changes and damage to the cellular membranes. Outer membrane of Gram-negative bacteria is composed of lipopolysaccharide in addition to a thin peptidoglycan layer and acts as a primary permeability barrier for macromolecules and hydrophobic drugs. However, for Gram-positive bacteria, the structure is rather simple as they have a membrane, which surrounds the cell, and a cell wall primarily made up of peptidoglycan layer as well as teichoic and lipoteichoic acids. Still date, the mechanism of antimicrobial activity of NiO is not understood. For both cases due to direct contact, NiO nanoparticles damaged the cell membrane. The global charge of the bacterial cell at physiological pH was negative due to the dissociation of excess carboxylic groups at the cell surface [33, 34]. Since NiO has a positive surface charge and a $\zeta = 36.8 \pm 0.9$ mV (found from Zeta potential measurement), they became electrostatically bound to the negative cell surface hindering the cell activity. Penetration of NiO into the cell and its toxicity made it inactive and dead followed by lysis [35].Some studies suggest that the small size of nanoparticles is a factor in penetrating the bacteria membrane. It was reported that the outer cell membranes have pores in the nanometer range, and that nanoparticles which are smaller than the diameter of the pores can penetrate the

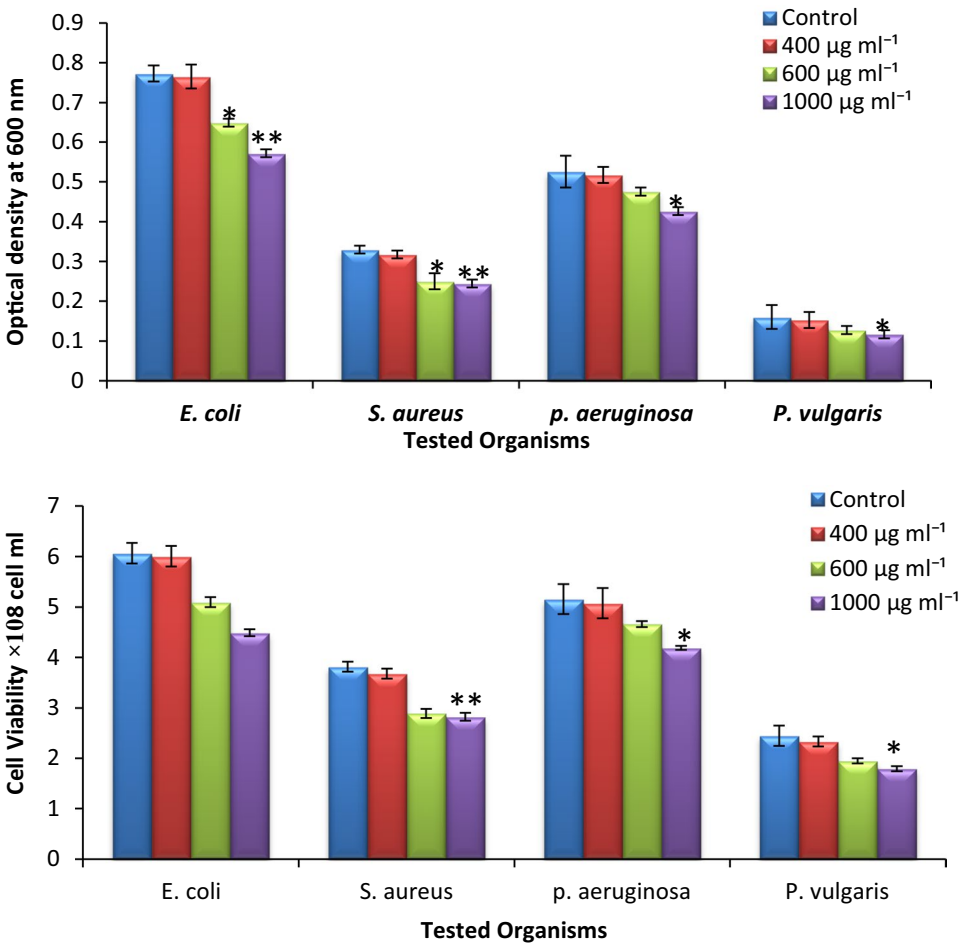

Fig. 7 Growth curves of tested organisms in broth in the presence of NiO nanoparticles: **a** optical density at 600 nm and **b** cell viability. *Error bars* are *≤0.05, **≤0.1

cell membrane [18]. This results in uncontrolled mass transfer through the membranes [36]. As a result, the nanoparticles damage the cell membranes as a result of reactive oxygen species (ROS), such as superoxide (O^{2-}) and hydroxyl (OH^{-}) radicals or direct cell damage. For metal-oxide nanoparticles, superoxide and hydroxyl radicals are two ROS produced by metal-oxide nanoparticles that cause cell damage. ROS oxidise double bonds in phospholipids, leading to increased membrane fluidity which leaves cells more susceptible to osmotic stress. ROS can also damage iron-sulphur clusters that function as cofactors in enzymes. Bactericidal activity of such nanoparticles is influenced by the size, concentration, and stability of nanoparticles in the growth medium [37].

Figure 8 shows the suppressive effect of amoxicillin (30 µg ml^{-1}) against *E. coli* and *S. aureus* with and without NiO nanoparticles. The concentration of NiO nanoparticles in each case was 400, 600, and 1000 µg ml^{-1}. The optical density of the bacterial cultures decreased as the concentrations of nanoparticles combined with amoxicillin were increased. This result proved that the antibacterial effect of amoxicillin improved in the presence of the NiO nanoparticles; this effect was the strongest at the highest concentration (1000 µg ml^{-1}) against both bacteria strains. The small size of the nanoparticles provides a large surface area for interaction with the bacterial cells. Such a large contact surface enhances the extent of bacterial elimination. When nanoparticles and antibiotics are used together, they have an extremely strong effect against Gram-positive and Gram-negative bacteria. The combined effect of metal-oxide nanoparticles and amoxicillin may be caused by lysis induced by the amoxicillin and the DNA-binding action of the nanoparticles. The antibiotic molecules contain many active groups, such as hydroxyl and amino groups, which reacts easily with nanoparticles by chelation. Thus, the synergistic effect may be due to the bonding reaction between the antibiotics and the nanoparticles [38]. Another mechanism reported by Tiwari et al. [39] is the existence of hydrophobic groups, such as phospholipids and glycoprotein, in the bacteria cell membrane which give the nanoparticles hydrophobic properties. In contrast, amoxicillin is hydrophilic, and can easily approach the membrane of the bacteria cells. As a result, the antimicrobial groups can easily transfer the amoxicillin to the cell surface [39]. This new idea was developed to counteract the incidence of high bacterial resistance to different antibiotics.

Figure 9 shows the inhibition rate of pure amoxicillin, pure NiO_2 nanoparticles, and a mixture of the two against *E.coli* and *S. aureus* bacteria. In the case of the pure amoxicillin, the inhibitory rate was about 74.8 and 76.28% against *E.coli* and *S. aureus*, respectively. This figure was enhanced to 81.5% against *E.coli* and 86.9% against *S. aureus* in the case of NiO nanoparticles with amoxicillin. It can be concluded that the efficiency of inhibiting bacterial growth could be improved by the addition of metal-oxide nanoparticles to amoxicillin in comparison with either pure amoxicillin or pure metal-oxide nanoparticles.

The synergistic antibacterial activity of the NiO nanoparticles combined with amoxicillin was also tested against *E. coli* and *S. aureus* using the well-diffusion method. Figure 10 shows the inhibition zone (IZ) results against *E. coli* and *S. aureus* bacteria. It can be noted that the nanoparticles enhanced the antibacterial activity of amoxicillin. It is worth mentioning that higher concentrations of the synthesised metal-oxide nanoparticles exhibited the best results along with amoxicillin.

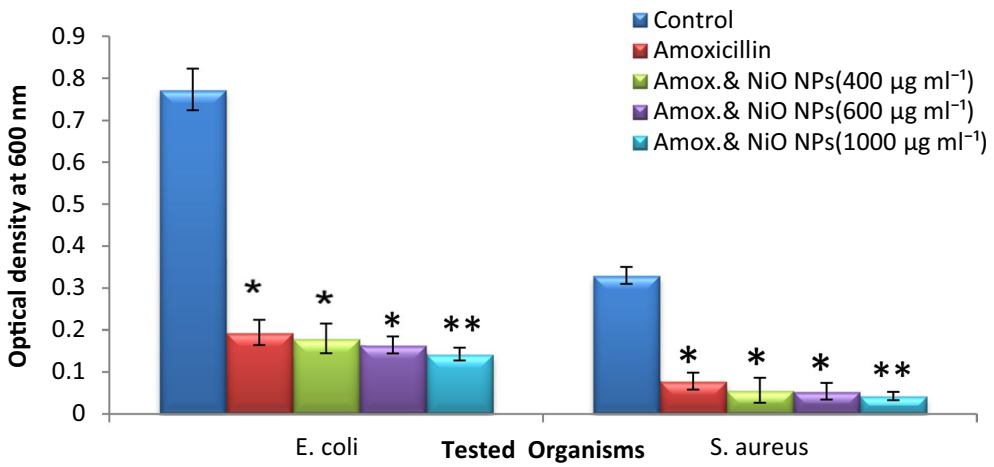

Fig. 8 Optical density (OD_{600}) of amoxicillin and NiO nanoparticles in LB medium against *E. coli* and *S. aureus*. The amoxicillin concentration was 30 µg ml^{-1} and the concentrations of the nanoparticles were 400, 600, and 1000 µg ml^{-1}. *Error bars* are *≤0.05, **≤0.1

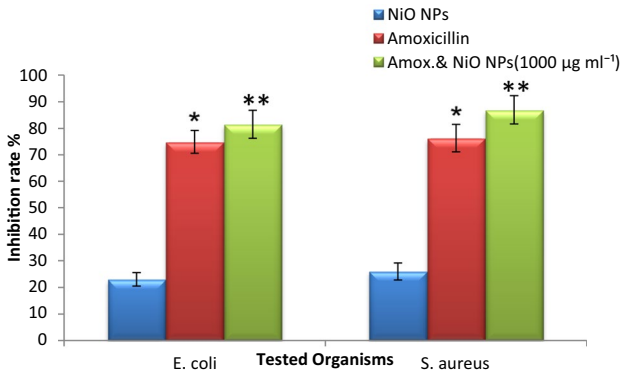

Fig. 9 Inhibition rate (%) of tested bacteria after treatment with amoxicillin or nanoparticles separately and amoxicillin together with NiO nanoparticles against *E. coli* and *S. aureus. Error bars* are *≤0.05, **≤0.1

The synergetic effect of NiO nanoparticles combined with amoxicillin was observed by the increase in inhibition zones (mm). As shown in Table 2, the highest increase in the inhibition zones was observed for a 1000 µg ml^{-1} concentration of NiO nanoparticles with amoxicillin. Nanoparticles are important, because their large surface area allows them to carry a large number of antibiotics. More antibiotic molecules can then be absorbed on the surface of the nanoparticles. The nanoparticles are surrounded by a number of antibiotics, which then act as a single group against the microorganisms. Such a group can then effectively bind to the outer membrane of the organisms. This synergistic effect may be attributed to the reaction between the antibiotics and the nanoparticles. Antibiotic molecules contain groups, such as hydroxyl groups, which may easily react with nanoparticles. Therefore, nanoparticles function as an antibiotic carrier in addition to their antibacterial properties.

Table 2 Inhibition zone of NiO nanoparticles with amoxicillin against *E. coli* and *S. aureus*

Organism	Concentration	Inhibition zone (mm)
E. coli	Control (Amoxicillin)	9.3 ± 0.57
	400 µg ml^{-1}	9.6 ± 0.57
	600 µg ml^{-1}	11.6 ± 0.57
	1000 µg ml^{-1}	14.3 ± 1.15
S. aureus	Control (Amoxicillin)	9.6 ± 0.57
	400 µg ml^{-1}	10.6 ± 0.57
	600 µg ml^{-1}	11.0 ± 1.00
	1000 µg ml^{-1}	12.6 ± 0.57

4 Conclusion

Pulsed laser ablation in a liquid environment is an efficient method to synthesise colloidal NiO nanoparticles. Nickel oxide (NiO) nanoparticles were generated by nanosecond laser in deionised water. They have a spherical shape with high aggregation. The absorption spectrum of NiO nanoparticles showed increasing absorption peaks with increasing laser energy and ablation time. The antibacterial activity of the nanoparticles increased with increasing nanoparticle concentration. Their optimal antibacterial activity was observed against *P. vulgaris*. In addition, NiO nanoparticles and amoxicillin were found to have a synergic effect on bacterial cells, and it was observed that nanoparticles can efficiently enhance the permeation and uptake of amoxicillin into bacteria cells. The antibacterial activity of NiO nanoparticles combined with amoxicillin in the solid medium agreed with results obtained using the liquid medium. NiO nanoparticles showed an inhibition zone against *E. coli* equal to 14.3 ± 1.15, and against *S. aureus*, this figure, was 12.6 ± 0.57. Thus, our findings concluded that the efficiency of inhibiting bacterial growth could be improved by the addition of NiO nanoparticles to

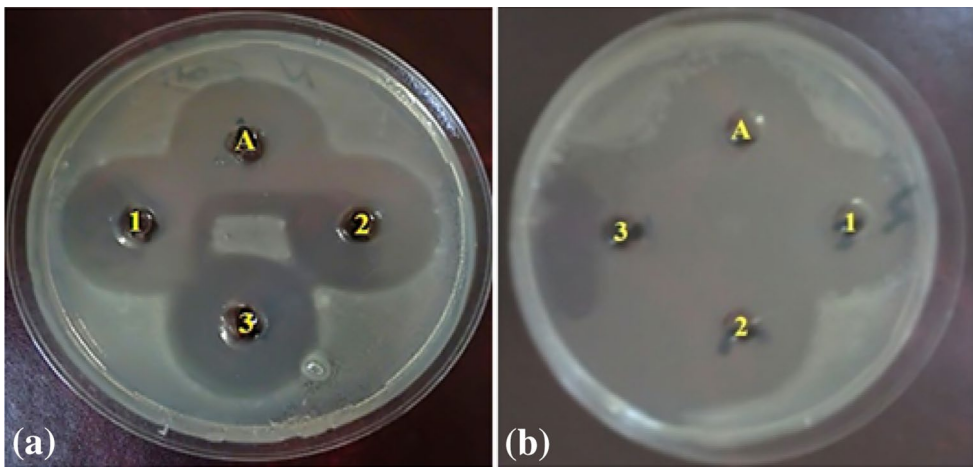

Fig. 10 Antimicrobial activity of NiO nanoparticles with amoxicillin (30 µg ml^{-1}) against **a***E. coli* and **b***S. aureus*, where *A* represents amoxicillin and *1, 2*, and *3* represent nanoparticles with concentrations of 400, 600, and 1000 µg ml^{-1}, respectively

amoxicillin in comparison with either pure amoxicillin or pure NiO nanoparticles.

Acknowledgements This work was supported by the Department of Applied Science, University of Technology, Baghdad, Iraq.

References

1. R. Tilaki, S. Mahdavi, Size, composition and optical properties of copper nanoparticles prepared by laser ablation in liquids. Appl. Phys. A **88**(2), 415–419 (2007)
2. G. Ren, D. Hu, E.W. Cheng, M.A. Vargas-Reus, P. Reip, R.P. Allaker, Characterisation of copper oxide nanoparticles for antimicrobial applications. Int. J. Antimicrob Agents **33**(6), 587–590 (2009)
3. N. Tarasenko, V. Burakov, A. Butsen, Laser ablation plasmas in liquids for fabrication of nanosize particles. Publications de l'Observatoire Astronomique de Beograd **82**, 201–211 (2007)
4. K.S. Khashan, G.M. Sulaiman, F.A. Abdulameer, Synthesis and antibacterial activity of CuO nanoparticles suspension induced by laser ablation in liquid. Arabian J. Sci. Eng. 41(1), 301–310 (2016)
5. C. Petridis, K. Savva, E. Kymakis, E. Stratakis, Laser generated nanoparticles based photovoltaics. J. Colloid Interface Sci. (2016). doi:10.1016/j.jcis.2016.09.065
6. S. Emmanuel, E.L. Kymakis, Nanoparticle-based plasmonic organic photovoltaic devices. Mater. Today **16**(4), 133–146 (2013)
7. T. Donnelly, S. Krishnamurthy, K. Carney, N. McEvoy, J. Lunney, Pulsed laser deposition of nanoparticle films of Au. Appl. Surf. Sci. **254**(4), 1303–1306 (2007)
8. P. Mallick, S. Sahu, Structure, microstructure and optical absorption analysis of CuO nanoparticles synthesized by sol-gel route. Nanosci. Nanotechnol. **2**(3), 71–74 (2012)
9. W.-N. Wang, I.W. Lenggoro, Y. Terashi, T.O. Kim, K. Okuyama, One-step synthesis of titanium oxide nanoparticles by spray pyrolysis of organic precursors. Mater. Sci. Eng. B **123**(3), 194–202 (2005)
10. K. Anandan, V. Rajendran, Morphological and size effects of NiO nanoparticles via solvothermal process and their optical properties. Mater. Sci. Semicond. Process. **14**, 43–47 (2011)
11. Y.D. Wang, C.L. Ma, X.D. Sun, H.D. Li, Preparation of nanocrystalline metal oxide powders with the surfactant mediated method. Inorg. Chem. Commun **5**, 751–755 (2002)
12. C. Coudun, J.F. Hochepied, Nickel hydroxide stacks of pancakes obtained by the coupled effect of ammonia and template agent. J. Phys. Chem B **109**, 6069–6074 (2005)
13. Z. Yan, R. Bao, D.B. Chrisey, Generation of Ag–Ag_2O complex nanostructures by excimer laser ablation of Ag in water. Phys. Chem. Chem. Phys. **15**, 3052–3056 (2013)
14. E.P. Mikhail, T.E. Itina, P.R. Levashovab, K.V. Khishchenko, Mechanisms of nanoparticle formation by ultra-short laser ablation of metals in liquid environment. Phys. Chem. Chem. Phys. **15**, 3108–3114 (2013)
15. A. Vincenzo, M. Meneghetti, What controls the composition and the structure of nanomaterials generated by laser ablation in liquid solution? Phys. Chem. Chem. Phys. **15**, 3027–3046 (2013)
16. N. Acacia, F. Barreca, E. Barletta, D. Spadaro, G. Currò, F. Neri, Laser ablation synthesis of indium oxide nanoparticles in water. Appl. Surf. Sci. **256**(22), 6918–6922 (2010)
17. N.M. Hosny, Synthesis, characterization and optical band gap of NiO nanoparticles derived from anthranilic acid precursors via a thermal decomposition route. Polyhedron **30**(3), 470–476 (2011)
18. D. Mohammadyani, S. Hosseini and S. Sadrnezhaad. Characterization of nickel oxide nanoparticles synthesized via rapid microwave-assisted route. *in International Journal of Modern Physics: Conference Series*. 2012: World Scientific
19. S. Jadhav, S. Gaikwad, M. Nimse, A. Rajbhoj, Copper oxide nanoparticles: synthesis, characterization and their antibacterial activity. J. Cluster Sci. **22**(2), 121–129 (2011)
20. Z. Emami-Karvani, P. Chehrazi, Antibacterial activity of ZnO nanoparticle on gram-positive and gram-negative bacteria. Afr. J. Microbiol. Res. **5**(12), 1368–1373 (2011)
21. M. Horie, K. Nishio, K. Fujita, H. Kato, A. Nakamura, S. Kinugasa, S. Endoh, A. Miyauchi, K. Yamamoto, H. Murayama, Ultrafine NiO particles induce cytotoxicity in vitro by cellular uptake and subsequent Ni(II) release. Chem. Res. Toxicol. **22**(8), 1415–1426 (2009)
22. A. Azam, A.S. Ahmed, M. Oves, M. Khan, A. Memic, Size-dependent antimicrobial properties of CuO nanoparticles against Gram-positive and-negative bacterial strains. Int. J. Nanomed. **7**(9), 3527–3535 (2012)
23. R. Swarnkar, S. Singh, R. Gopal, Effect of aging on copper nanoparticles synthesized by pulsed laser ablation in water: structural and optical characterizations. Bull. Mater. Sci. **34**(7), 1363–1369 (2011)
24. S.A. Mahdy, Q.J. Raheed, P. Kalaichelvan, Antimicrobial activity of zero-valent iron nanoparticles. Int. J. Mod. Eng. Res. **2**(1), 578–581 (2012)
25. D. Rosická, J. Šembera, Changes in the nanoparticle aggregation rate due to the additional effect of electrostatic and magnetic forces on mass transport coefficients. Nanoscale Res. Lett. **8**(1), 1–9 (2013)
26. G. Yang, Laser ablation in liquids: principles and applications in the preparation of nanomaterials. (Singapore, Pan Stanford Publishing, 2012)
27. R. Mahfouz, F.C.S. Aires, A. Brenier, B. Jacquier, J. Bertolini, Synthesis and physico-chemical characteristics of nanosized particles produced by laser ablation of a nickel target in water. Appl. Surf. Sci. **254**(16), 5181–5190 (2008)
28. C. Sima, C. Viespe, C. Grigoriu, G. Prodan, V. Ciupina, Production of oxide nanoparticles by pulsed laser ablation. J. Optoelectron. Adv. Mater. **10**(10), 2631–2636 (2008)
29. M. Salavati-Niasari, F. Davar, Z. Fereshteh, Synthesis of nickel and nickel oxide nanoparticles via heat-treatment of simple octanoate precursor. J. Alloys Compd. **494**(1), 410–414 (2010)
30. M. Gondal, T.A. Saleh, Q. Drmosh, Synthesis of nickel oxide nanoparticles using pulsed laser ablation in liquids and their optical characterization. Appl. Surf. Sci. **258**(18), 6982–6986 (2012)
31. K. Wolter, O. Seiferth, J. Libuda, H. Kuhlenbeck, M. Bäumer, H.-J. Freund, Infrared study of CO adsorption on alumina supported palladium particles. Surf. Sci. **402**, 428–432 (1998)
32. R. Gopal, M. Singh, A. Agarwal, S. Singh, R. Swarnkar, *Synthesis of nickel nanomaterial by pulsed laser ablation in liquid medium and its characterization*. in *AIP Conf Proc*. 2009
33. P.J.P. Espitia,, N. de F. F. Soares, J. S. dos R. Coimbra, N.J. de Andrade, R.S. Cruz, E.A.A. Medeiros, Zinc oxide nanoparticles: synthesis, antimicrobial activity and food packaging application. Food Bioprocess Technol **5**(5), 1447–1464 (2012)
34. S. Rakshit, S. Ghosh, S. Chall, S.S. Mati, S.P. Moulik, S.C. Bhattacharya, Controlled synthesis of spin glass nickel oxide nanoparticles and evaluation of their potential antimicrobial activity: a cost effective and eco friendly approach. RSC Adv. **3**, 19348–19356 (2013)
35. Stoimenov, P. K., R. L. Klinger, G. L. Marchin, K. J. Klabunde, Metal Oxide Nanoparticles as Bactericidal Agents, Langmuir **18**, 6679–6686 (2002).

36. T.M. Al-Nori, Antibacterial activity of Silver and Gold Nanoparticles against *Streptococcus, Staphylococcus aureus* and *E.coli*. Al-Mustansiriya J. Sci. **23**(3), 10 (2012)
37. Murthy, P.S., V. Venugopalan, D.A. Das, S. Dhara, R. Pandiyan, A. Tyagi. Antibiofilm activity of nano sized CuO. in *Nanoscience, Engineering and Technology (ICONSET), 2011 International Conference on IEEE* (2011)
38. S. Rajawat, M.S. Qureshi, Comparative study on bactericidal effect of silver nanoparticles, synthesized using green technology, in combination with antibiotics on *Salmonella typhi*. J. Biomater. Nanobiotechnol. **3**(4), 480 (2012)
39. D.K. Tiwari, J. Behari, P. Sen, Appl. Nanopart. Waste Water Treat. 1 (2008)